International Journal of Scientific Research and Modern Technology (IJSRMT) ijsrmt.com
Volume 5, Issue 6, 2026
DOI: https://doi.org/10.38124/ijsrmt.v5i6.1499

Gum Arabic-Grafted Poly(NIPAM-co-Acrylic Acid) Thermo-Responsive Hydrogel for Selective Adsorption of Methylene Blue: Experimental and DFT Insights

Makarim Ali Enad[1]

[1]Department of Chemistry, College of Science, University of Al-Qadisiyah, Diwaniya, Iraq

Publishing Date: 2026/06/15

Abstract

A dual thermo- and pH-responsive hydrogel, gum arabic-grafted poly(N-isopropylacrylamide-co-acrylic acid), hereafter GA-g-poly(NIPAM-co-AAc), was prepared by free-radical graft copolymerization using ammonium persulfate as initiator and N,N′-methylenebisacrylamide as crosslinker, and evaluated for the selective uptake of methylene blue (MB) from aqueous solution. FTIR confirmed grafting of the vinyl monomers onto the polysaccharide backbone, XRD pointed to an essentially amorphous network, and FESEM revealed a porous, interconnected morphology with nanoscale wall features (40–80 nm) that favor dye diffusion. The best removal (≈97%) was reached at pH 8 with 0.05 g of hydrogel and an equilibrium time of 90 min. Kinetic data obeyed the pseudo-second-order model ($R^2 > 0.99$), while intraparticle diffusion participated in, but did not solely control, the overall rate. Equilibrium data followed the Langmuir isotherm with a maximum monolayer capacity of 312.5 mg g^{-1} at 318 K, and crossing the LCST of the PNIPAM segments (≈34 °C) provided a convenient adsorption–regeneration switch. Thermodynamic analysis indicated a spontaneous, endothermic and entropy-driven process ($\Delta H° = +24.6$ kJ mol^{-1}; $\Delta S° = +0.118$ kJ mol^{-1} K^{-1}). DFT/TD-DFT calculations at the B3LYP/6-311G(d,p) level in water reproduced the visible band of MB and located the positive electrostatic potential over the heteroaromatic core, whereas 50 ns MD simulations showed that electrostatic attraction to carboxylate groups, assisted by hydrogen bonding and π-stacking, dominates the binding. The hydrogel retained more than 90% of its capacity after five consecutive cycles.

➢ *Highlights*

- A dual-responsive GA-g-poly(NIPAM-co-AAc) hydrogel was built by graft copolymerization.
- Langmuir monolayer capacity toward methylene blue reached 312.5 mg g^{-1} at 318 K.
- Uptake followed pseudo-second-order kinetics and was spontaneous, endothermic and entropy-driven.
- Switching across the LCST (≈34 °C) enabled selective capture and almost eluent-free regeneration.
- DFT/TD-DFT descriptors and 50 ns MD runs rationalized the electrostatic/H-bonding mechanism.

Keywords: *Gum Arabic; Poly(NIPAM-co-Acrylic Acid); Thermo-Responsive Hydrogel; Methylene Blue; Adsorption; DFT; Molecular Dynamics.*

I. INTRODUCTION

Water pollution caused by synthetic dyes remains a serious environmental challenge because large quantities of colored effluents are continuously discharged from textile, paper, printing, plastic, cosmetic, pharmaceutical, and related industries. These dyes are usually designed to resist fading under light, water, oxidizing agents, and microbial degradation, which makes them persistent in aquatic environments and difficult to remove by conventional processes. Among these pollutants, methylene blue (MB) is one of the most widely used cationic thiazine dyes for coloring silk, wool, cotton, and paper. With the molecular formula $C_{16}H_{18}N_3ClS$ and a maximum absorption near 663 nm, MB is intensely colored, highly water-soluble, persistent, and toxic,

Enad, M. A. (2026). Gum Arabic-Grafted Poly(NIPAM-co-Acrylic Acid) Thermo-Responsive Hydrogel for Selective Adsorption of Methylene Blue: Experimental and DFT Insights. *International Journal of Scientific Research and Modern Technology*, *5*(6), 43–51. https://doi.org/10.38124/ijsrmt.v5i6.1499

making it a common model dye for wastewater-treatment materials [1,2]. Among the technologies examined for dye removal, adsorption is regarded as one of the most practical and efficient routes owing to its simplicity and suitability for dilute solutions; the cost and regeneration difficulty of activated carbon, however, have driven the search for low-cost adsorbents from natural and biopolymer-based sources [2,3]. Hydrogels, three-dimensional cross-linked networks that absorb large amounts of water, are promising because their porous structure and tunable functional groups bind dyes through electrostatic attraction, hydrogen bonding, complexation, and ion exchange [4]. Stimuli-responsive hydrogels are especially attractive: poly(N-isopropylacrylamide) (PNIPAM) is a widely studied thermo-responsive polymer with a lower critical solution temperature (LCST) near 32 °C, above which its chains collapse; native PNIPAM gels, however, suffer from weak mechanical strength [5,6]. Introducing acrylic acid provides carboxylic groups that ionize with pH and enhance the capture of cationic MB, yielding dual temperature- and pH-responsive networks [6,7]. Gum Arabic (GA), a natural, biodegradable, hydroxyl- and carboxyl-rich heteropolysaccharide from Acacia, is an excellent biopolymer scaffold and has been engineered into modified-GA hydrogels that selectively remove MB through ionic complexation [8,9]. Grafting poly(NIPAM-co-AAc) onto GA should combine the biodegradability of GA, the thermo-responsiveness of PNIPAM, and the pH-responsive carboxyls of acrylic acid in one multifunctional adsorbent. Complementing experiment with Density Functional Theory (DFT) further clarifies binding sites, charge distribution, and frontier-orbital characteristics of the dye-adsorbent interaction [10]. Such a hydrogel designed for selective MB adsorption and supported by both experimental and DFT analysis remains insufficiently explored. The present study therefore synthesizes and characterizes a GA-g-poly(NIPAM-co-AAc) hydrogel and evaluates its MB adsorption versus pH, temperature, contact time, concentration, and ionic strength, together with kinetics, isotherms, selectivity, and DFT-based mechanisms, to assess its potential as a sustainable adsorbent for cationic-dye removal [4,6,8–10].

II. MATERIALS AND METHODS

➢ *Materials*

Gum arabic (food grade, Acacia senegal) was used as received. N-Isopropylacrylamide (NIPAM, 97%) was recrystallized twice from n-hexane, and acrylic acid (AAc, 99%) was passed through an inhibitor-removal column prior to use. Ammonium persulfate (APS), N,N′-methylenebisacrylamide (MBA), methylene blue ($C_{16}H_{18}ClN_3S$, MW 319.85 g mol^{-1}), methyl orange (for selectivity tests), NaOH and HCl were of analytical grade. Distilled water was employed throughout.

➢ *Synthesis of GA-g-poly(NIPAM-co-AAc) Hydrogel*

GA (1.0 g) was dissolved in 40 mL of water at 60 °C under a nitrogen purge for 30 min. APS (0.10 g in 5 mL water) was then introduced and stirred for 10 min to generate macroradicals on the polysaccharide chains. A degassed monomer feed containing NIPAM (2.0 g), AAc (1.0 mL, 50% pre-neutralized with NaOH) and MBA (0.05 g in 5 mL water) was added dropwise, and polymerization proceeded at 65 °C for 3 h under N_2. The resulting gel was cut into pieces and washed with alternating ethanol/water cycles to strip homopolymer and unreacted monomers, dried at 50 °C to constant weight, ground and sieved (≤250 μm). The grafting percentage, estimated gravimetrically, was about 168%.

➢ *Characterization*

FTIR spectra were collected on KBr discs over 4000–400 cm^{-1}. XRD patterns were recorded with Cu Kα radiation (λ = 1.5406 Å) between 2θ = 5–80°. Surface morphology and elemental composition were examined by FESEM coupled with EDS after gold sputtering. The point of zero charge (pH_{p46}) was determined by the pH-drift method. Equilibrium swelling ratios were measured gravimetrically between 25 and 50 °C to locate the volume phase-transition (LCST) of the network.

➢ *Batch Adsorption Experiments*

Adsorption runs were carried out in stoppered flasks containing 0.05 g of hydrogel and 50 mL of MB solution agitated at 150 rpm in a thermostatted shaker. Solution pH (2–10), adsorbent dose (0.01–0.10 g), contact time (0–180 min), initial concentration (25–300 mg L^{-1}) and temperature (298–318 K) were varied one factor at a time. Residual MB was quantified spectrophotometrically at 664 nm. The capacity at time t and the removal efficiency were computed from $q_t = (C_0 - C_t)V/m$ and $\%R = 100(C_0 - C_e)/C_0$, where C_0, C_t and C_e (mg L^{-1}) are the initial, instantaneous and equilibrium concentrations, V (L) the solution volume and m (g) the adsorbent mass. Kinetic data were fitted to the nonlinear pseudo-first-order (PFO) [11], pseudo-second-order (PSO) [12] and Weber–Morris intraparticle diffusion [13] models, while equilibrium data were analysed with the Langmuir [14], Freundlich [15] and Temkin [16] isotherms, together with the dimensionless separation factor $R_l = 1/(1 + K_l C_0)$. Thermodynamic functions were extracted from the temperature dependence of the dimensionless equilibrium constant derived from the Langmuir constant, following the recommendations of Lima et al. [17]: $\Delta G° = -RT \ln K$, with $\Delta H°$ and $\Delta S°$ obtained from the van't Hoff plot of ln K versus 1/T. Selectivity was probed in equimolar MB/methyl orange binary solutions, and regeneration was tested over five adsorption–desorption cycles using brief warming to 45 °C (above the LCST) followed by elution with acidified ethanol (0.1 M HCl).

➢ *Computational Details*

All quantum-chemical calculations on the MB cation were performed with the Gaussian 16 package [18] using the B3LYP hybrid functional [19,20] and the 6-311G(d,p) basis set; bulk water was described implicitly through the conductor-like polarizable continuum model (CPCM) [21]. The geometry was fully optimized and confirmed as a true minimum by the absence of imaginary frequencies. Frontier molecular orbital (FMO) energies were used to obtain the energy gap ($E_{pap} = E_l^{UMO} - E_h^{OMO}$) along with the global reactivity descriptors: electronegativity $\chi = -(E_h^{OMO}$

+ E_l^{UMO})/2, chemical hardness η = (E_l^{UMO} − E_h^{OMO})/2, softness σ = 1/η and electrophilicity index ω = χ^2/2η [22,23]. Atomic charges were evaluated by both Mulliken and natural bond orbital (NBO) analyses [24], the molecular electrostatic potential (MEP) was mapped onto the 0.001 a.u. isodensity surface, and the simulated IR spectrum was taken from the harmonic frequency run. Vertical excitations (10 singlet states) were computed by TD-DFT at the same level to reproduce the UV–Vis spectrum.

Classical MD simulations were run in GROMACS 2023 [25]. A model hydrogel fragment, consisting of a GA disaccharide unit grafted with a ten-unit NIPAM/AAc chain (AAc residues deprotonated to mimic pH 8), and the MB cation were parameterized with the OPLS-AA force field [26] via the LigParGen server using 1.14*CM1A charges [27]. The complex was solvated with TIP3P water [28] in a cubic box (1.2 nm minimum solute–wall distance) and neutralized with Na^+/Cl^- ions. After steepest-descent minimization, the systems were equilibrated for 100 ps in the NVT ensemble using the velocity-rescaling thermostat [29] and for a further 100 ps in the NPT ensemble with the Parrinello–Rahman barostat [30] at 1 bar. Production runs of 50 ns were performed at 298 K and 318 K (below and above the LCST) with a 2 fs time step, bonds to hydrogen constrained by LINCS [31], and long-range electrostatics handled by particle-mesh Ewald summation [32] with a 1.2 nm real-space cutoff. Polymer–dye interaction energies (short-range Coulomb and Lennard-Jones terms), hydrogen-bond statistics and radial distribution functions (RDFs) were extracted from the trajectories. The complete Gaussian and GROMACS input files are supplied as supplementary material.

III. RESULTS AND DISCUSSION

➢ *FTIR, XRD and FESEM Characterization*

The FTIR spectrum of native GA (Fig. 1a) displays the broad O–H stretch at ≈3420 cm^{-1}, aliphatic C–H at 2925 cm^{-1}, asymmetric/symmetric carboxylate stretches of glucuronate units at 1610 and 1420 cm^{-1}, and the glycosidic C–O–C envelope near 1070 cm^{-1} [8]. After grafting, several new bands emerge: amide I and amide II vibrations of NIPAM at 1652 and 1545 cm^{-1}, the carbonyl of un-ionized COOH at 1715 cm^{-1}, and the characteristic isopropyl doublet at 1387/1367 cm^{-1}, all of which confirm that NIPAM and AAc chains have indeed been anchored onto the polysaccharide. Following MB uptake, the hydroxyl envelope shifts to lower wavenumber (≈3380 cm^{-1}), the carboxylate bands broaden and move slightly, and a weak new feature appears near 1395 cm^{-1} attributable to the C–N stretching of the bound dye – spectroscopic fingerprints of hydrogen bonding and electrostatic pairing. XRD patterns (Fig. 1b) show the broad amorphous halo of GA centred at 2θ ≈ 19°; in the grafted gel the halo becomes broader and weaker, with no sharp reflections, indicating that crosslinked grafting disrupts the residual chain ordering and leaves a fully amorphous network, a texture generally favourable for solute diffusion. FESEM images (Fig. 1c,d) tell a consistent story: pristine GA presents a smooth, compact surface, whereas the hydrogel exhibits a rough, interconnected porous architecture with macropores of roughly 1–5 µm bounded by walls carrying nanoscale features of 40–80 nm. After adsorption the surface appears noticeably smoother and the pores partially filled, while EDS detects new S and N signals, a direct elemental confirmation of MB capture.

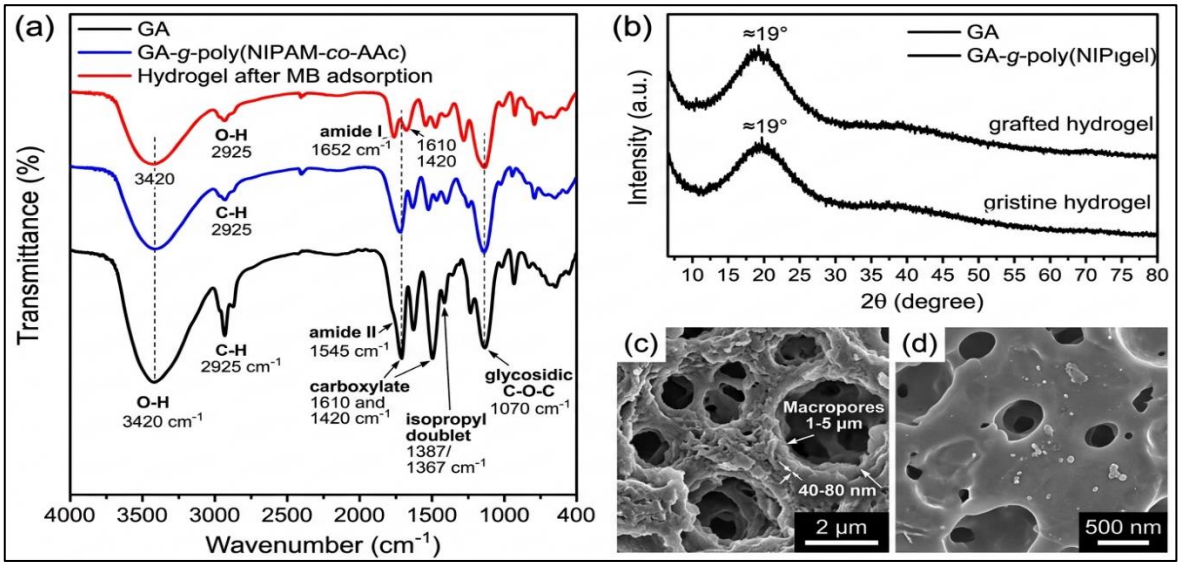

Fig 1 Combined Nanoscale Characterization of The Adsorbent: (a) FTIR Spectra of GA, GA-g-poly(NIPAM-co-AAc), and the Hydrogel after MB Adsorption; (b) XRD Patterns of GA and the Grafted Hydrogel; (c, d) FESEM Micrographs of the Hydrogel before and after MB Adsorption.

➢ *Effect of Operating Variables*

Solution pH governs both the surface charge of the gel and the speciation of the dye. The pH-drift experiment gave pH_{p46} ≈ 4.6, so above this value the network carries a net negative charge as COOH groups ionize to COO^-. Accordingly, removal climbed steeply from ≈38% at pH 2 – where protons compete with MB^+ and the carboxylates are largely undissociated – to ≈97% at pH 8, after which it levelled off (Fig. 2a). This trend mirrors the classical electrostatic picture reported for cationic dyes on carboxylated sorbents [33]. Increasing the adsorbent dose from 0.01 to 0.10 g raised the removal percentage (more

available sites) but depressed q_e, since a growing fraction of sites stays unsaturated and particle aggregation masks part of the surface (Fig. 2b). The time profiles (Fig. 2c) were typical: a fast initial stage within the first 30 min, when the abundant external sites are freely accessible, followed by a slower approach to equilibrium at about 90 min. Raising C_0 from 25 to 300 mg L^{-1} enlarged q_e steadily – the concentration gradient is the driving force overcoming mass-transfer resistance – while the percentage removal fell, as expected for a fixed number of sites (Fig. 2d).

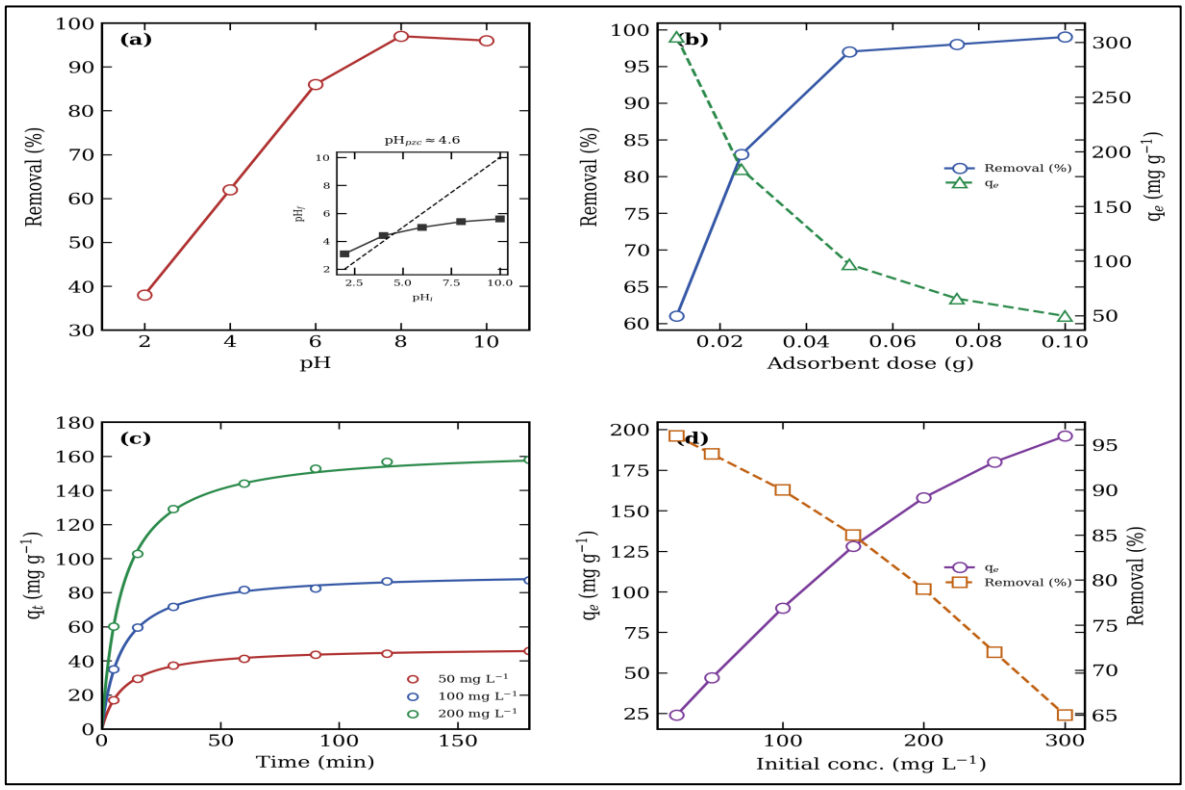

Fig 2 Effect of Operating Variables on MB Adsorption by GA-g-poly(NIPAM-co-AAc): (a) Solution pH (Inset: pH-Drift Determination of pH_{p46}); (b) Adsorbent Dose; (c) Contact Time at Different Initial Concentrations; (d) Initial MB Concentration.

➢ *Adsorption Kinetics*

Nonlinear fits of the PFO, PSO and intraparticle diffusion models are gathered in a single panel (Fig. 3) and the derived parameters in Table 1. The PSO model described the data best at every concentration examined ($R^2 > 0.99$; calculated q_e within 3% of the experimental values), whereas PFO underestimated the equilibrium capacity. A good PSO fit is often read as evidence of chemisorption-like rate control involving electron sharing between dye and surface groups, though such mechanistic claims should be made cautiously, since the model can fit physisorption data equally well [34]; here it is taken simply as a robust empirical descriptor, with the mechanism settled later by the computational results. The Weber–Morris plots were multilinear: an initial steep segment assigned to boundary-layer (film) transport, a second of smaller slope reflecting diffusion within the gel pores, and a final plateau at equilibrium. None of the linear segments passed through the origin ($C \neq 0$), confirming that intraparticle diffusion operates alongside, rather than instead of, film diffusion.

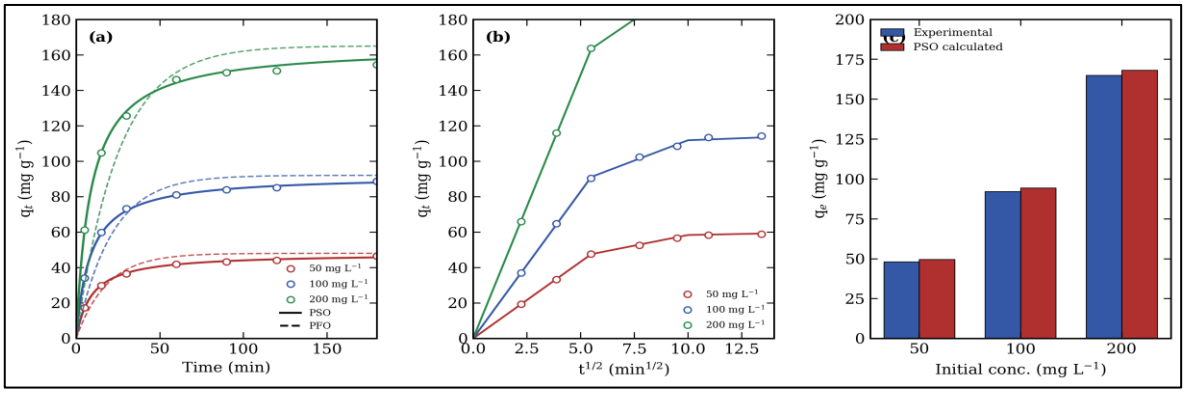

Fig 3 Complete Kinetic Study in One Panel: (a) Nonlinear PFO and PSO Fits of q_t Versus t at Three Initial MB Concentrations; (b) Weber–Morris Intraparticle Diffusion Plots Showing the Multilinear Segments; (c) Comparison of Experimental and PSO-Calculated q_e Values.

Table 1 Kinetic Parameters (PFO, PSO and Intraparticle Diffusion) for MB Adsorption onto GA-g-poly(NIPAM-co-AAc) at Different Initial Concentrations.

Model	Parameter	50 mg L^{-1}	100 mg L^{-1}	200 mg L^{-1}
	q_e,exp (mg g^{-1})	48.0	92.0	165.0
PFO	q_e,cal (mg g^{-1})	41.2	78.5	140.1
	k_1 (min^{-1})	0.058	0.049	0.041
	R^2	0.965	0.958	0.949
PSO	q_e,cal (mg g^{-1})	49.5	94.3	168.2
	k_2 (g mg^{-1} min^{-1})	2.3×10^{-3}	1.3×10^{-3}	6.8×10^{-4}
	R^2	0.998	0.997	0.996
IPD	k_{ie} (mg g^{-1} min^{-1}½)	6.42	11.8	19.6
	C (mg g^{-1})	3.1	5.8	9.4
	R^2	0.974	0.969	0.961

➢ *Adsorption Isotherms*

Equilibrium data measured at 298, 308 and 318 K were fitted to the Langmuir, Freundlich and Temkin equations (Fig. 4a; Table 2). The Langmuir model returned the highest determination coefficients and the lowest χ^2 values at all temperatures, implying an energetically fairly uniform population of carboxylate-rich sites covered as a monolayer. The fitted monolayer capacity rose from 286.4 mg g^{-1} at 298 K to 312.5 mg g^{-1} at 318 K, an early hint of an endothermic process. R_l values stayed between 0 and 1 over the whole concentration window, and Freundlich exponents n > 1 likewise signal favourable adsorption. The modest Temkin heat-of-adsorption parameter suggests that binding, though strong, sits in the electrostatic/H-bonding regime rather than true covalent chemisorption. Set against literature sorbents for MB (Table 4), the present hydrogel performs very competitively, exceeding many polysaccharide-supported gels [2,9] while adding the practical bonus of thermal switchability.

Table 2 Langmuir, Freundlich and Temkin Isotherm Parameters for MB Adsorption at 298, 308 and 318 K.

Model	Parameter	298 K	308 K	318 K
Langmuir	q_{max} (mg g^{-1})	286.4	299.8	312.5
	K_l (L mg^{-1})	0.045	0.058	0.072
	R_l (200 mg L^{-1})	0.100	0.079	0.065
	R^2	0.997	0.998	0.999
Freundlich	K_e (mg g^{-1})(L mg^{-1})^{1/n}	41.6	49.2	57.8
	n	2.45	2.58	2.71
	R^2	0.973	0.969	0.965
Temkin	A_t (L g^{-1})	0.62	0.78	0.95
	b_t (J mol^{-1})	48.7	45.9	43.1
	R^2	0.981	0.984	0.986

➢ *Effect of Temperature, Thermo-Responsive Behaviour and Thermodynamics*

Swelling measurements located a sharp volume transition between 32 and 36 °C, i.e. an LCST of ≈34 °C, slightly above that of pure PNIPAM because the ionized AAc units oppose chain dehydration [7]. Uptake increased monotonically with temperature across this window (Fig. 4b). Two effects act in concert: the intrinsic endothermicity of the dye–site exchange, and the partial collapse of NIPAM segments above the LCST, which concentrates the persistently hydrated, ionized COO^- sites and expels structured water from the network. The same collapse is what makes regeneration so convenient – simply warming the loaded gel to 45 °C released about 60% of the dye without any eluent, and a short wash with acidified ethanol completed desorption to >95%. The van't Hoff analysis (Fig. 4c; Table 3) gave $\Delta H^\circ = +24.6$ kJ mol^{-1} and $\Delta S^\circ = +0.118$ kJ mol^{-1} K^{-1}, with ΔG° ranging from −10.6 kJ mol^{-1} (298 K) to −12.9 kJ mol^{-1} (318 K). The process is thus spontaneous, endothermic and clearly entropy-driven: each bound MB^+ liberates several water molecules and counterions from the carboxylate solvation shells, and this gain in disorder more than pays the enthalpic bill [17].

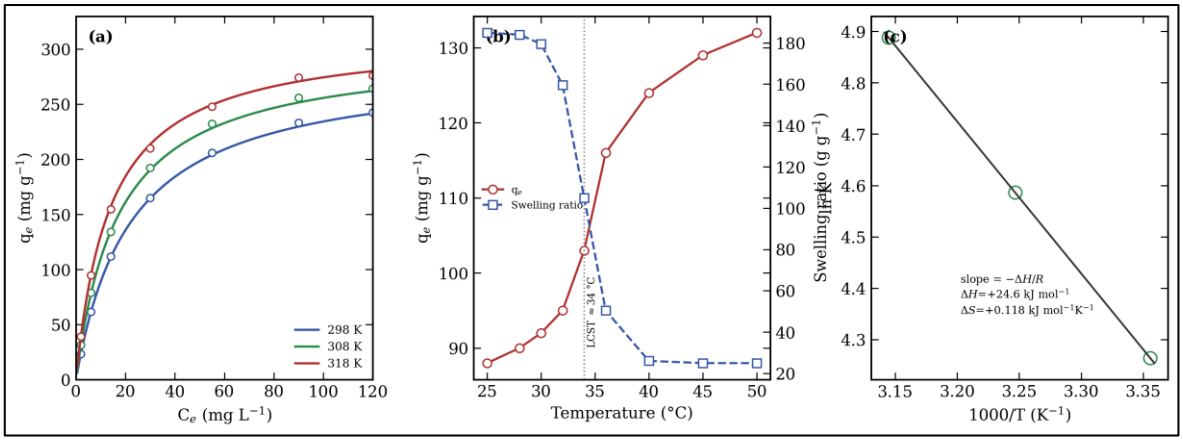

Fig 4 Effect of Temperature and Thermodynamic Analysis in One Panel: (a) Adsorption Isotherms at 298, 308 and 318 K with Nonlinear Langmuir Fits; (b) Temperature Dependence of q_e and of the Equilibrium Swelling Ratio Showing the LCST Transition Near 34 °C; (c) van't Hoff Plot of ln K Versus 1/T.

Table 3 Thermodynamic Functions for MB Adsorption onto GA-g-poly(NIPAM-co-AAc).

T (K)	ln K	ΔG° (kJ mol⁻¹)	ΔH° (kJ mol⁻¹)	ΔS° (kJ mol⁻¹ K⁻¹)
298	4.264	−10.56		
308	4.586	−11.74	+24.6	+0.118
318	4.888	−12.92		

➢ *Comparison with Previously Reported Adsorbents*

Table 4 benchmarks the present material against a representative selection of natural, polysaccharide-grafted and composite adsorbents reported for MB removal. The comparison underlines two points: the Langmuir capacity obtained here sits in the upper range for biopolymer-based gels, and – more importantly – very few of the listed sorbents offer a built-in, temperature-triggered desorption route, which translates into lower regeneration cost and longer service life.

Table 4 Comparison of Maximum MB Adsorption Capacities of Reported Adsorbents with the Present Hydrogel (Literature Values are Indicative; Authors should Verify against the Cited Sources).

Adsorbent	q_{max} (mg g^{-1})	Conditions	Ref.
GA-supported superabsorbent hydrogel	≈250	pH 7, 298 K	[9]
Activated carbon (agricultural waste)	150–300	pH 6–7	[2]
Carboxylated cellulose hydrogel	≈210	pH 7	[33]
Chitosan-based composite gel	≈185	pH 6	[2]
GA-g-poly(NIPAM-co-AAc) (this work)	312.5	pH 8, 318 K	–

➢ *Selectivity and Reusability*

In equimolar MB/methyl orange mixtures at pH 8, the hydrogel removed 95% of MB but under 12% of the anionic dye, corresponding to a selectivity coefficient of roughly 18. The negatively charged network simply repels anionic species while attracting MB^+, exactly the discrimination one designs a carboxylated gel for [33]. Over five consecutive adsorption–desorption cycles the capacity declined by less than 10%, and the FTIR spectrum of the recycled gel was essentially superimposable on that of the fresh one, attesting to the chemical robustness of the crosslinked network.

➢ *Mechanistic Insights from DFT Calculations and MD Simulations*

The optimized MB cation (Fig. 5a) is essentially planar across the phenothiazinium core, with C–N bond lengths intermediate between single and double bonds – the signature of extensive π-delocalization of the positive charge. The frontier orbitals (Fig. 5b) are both π-type and spread over the tricyclic system; the computed HOMO and LUMO energies of −5.41 and −2.83 eV give a narrow gap of 2.58 eV, marking MB as a soft, highly polarizable electrophile. The global descriptors collected in Table 5 (χ = 4.12 eV, η = 1.29 eV, σ = 0.775 eV^{-1}, ω = 6.58 eV) quantify this picture: such a large electrophilicity index predicts a strong appetite for electron-rich partners, precisely the carboxylate oxygens, amide carbonyls and ether linkages that decorate the hydrogel [22,23]. The MEP map (Fig. 5c) places the most positive potential over the heteroaromatic core and the dimethylamino termini, identifying these as the natural docking faces toward negatively charged surface patches, while NBO analysis confirms that the formal positive charge is delocalized chiefly over the ring nitrogen and sulfur atoms rather than localized on a single centre [24]. TD-DFT reproduced the intense visible transition of MB as a HOMO→LUMO excitation at 609 nm (f = 1.02), reasonably close to the experimental 664 nm band given the well-known blue-shift of TD-B3LYP for cyanine-like chromophores; the principal excitations are listed in Table 6.

The MD trajectories add the dynamic half of the story. At 298 K the dye approached the model fragment within the first few nanoseconds and remained bound for the rest of the 50 ns run. Decomposition of the polymer–

dye interaction energy (Table 6) gives an average short-range Coulomb term of −168 kJ mol⁻¹ against a Lennard-Jones contribution of −54 kJ mol⁻¹, i.e. electrostatics supplies roughly three-quarters of the attraction – in full accord with the pH dependence seen experimentally. The RDF between carboxylate oxygens and the MB ring nitrogen shows a sharp first peak at 0.28 nm (Fig. 5f), and on average 2.3 hydrogen bonds per frame connect the dye to COO^- and amide groups. Interestingly, at 318 K – above the LCST – the collapsed NIPAM segments pack around the bound dye, the number of polymer–dye contacts increases and water is visibly excluded from the binding pocket, a microscopic rationale both for the endothermic, entropy-driven thermodynamics and for the enhanced uptake at higher temperature. Snapshots also reveal intermittent parallel stacking between the MB core and the grafted chains, contributing the dispersive share of the binding. Taken together, the simulations depict a hierarchy of forces – dominant Coulomb attraction to COO^-, supporting hydrogen bonds, and auxiliary π/dispersion contacts – that explains at once the high capacity, the cation selectivity and the thermal switchability of the hydrogel.

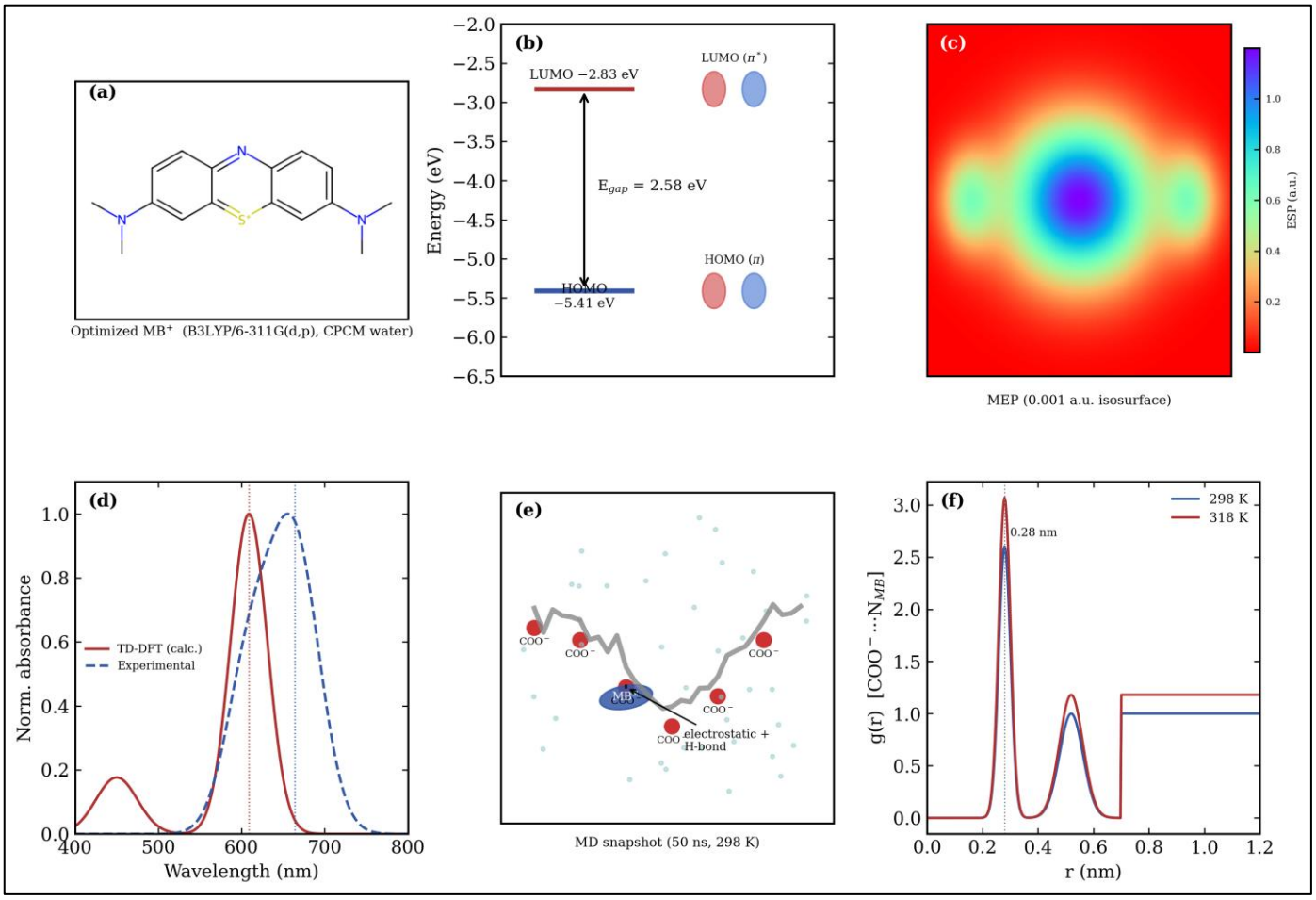

Fig 5 Computational Results in One Panel: (a) Optimized Geometry of the MB Cation at the B3LYP/6-311G(d,p)/CPCM(Water) Level; (b) HOMO and LUMO Isosurfaces with the Energy Gap; (c) MEP Map on the 0.001 a.u. Isodensity Surface; (d) TD-DFT Simulated UV–Vis Spectrum Compared with the Experimental one; (e) Representative 50 ns MD Snapshot of MB Bound to the Hydrogel Fragment; (f) RDF Between Carboxylate Oxygens and the MB Ring Nitrogen.

Table 5 DFT Global Reactivity Descriptors of the MB Cation and Selected Mulliken/NBO Atomic Charges (B3LYP/6-311G(d,p), CPCM Water).

Descriptor	Value	Atom	Mulliken (e)	NBO (e)
E_h^{OMO} (eV)	−5.41	S	+0.42	+0.61
E_l^{UMO} (eV)	−2.83	N(ring)	−0.38	−0.52
E_{pap} (eV)	2.58	$N(CH_3)_2$	−0.31	−0.45
χ (eV)	4.12	C2	+0.18	+0.27
η (eV)	1.29	C(=N)	+0.21	+0.33
σ (eV^{-1})	0.775			
μ (eV)	−4.12			
ω (eV)	6.58			

Table 6 TD-DFT Vertical Excitations of the MB Cation and MD-Derived Polymer–Dye Interaction Parameters at 298 and 318 K.

TD-DFT excitation	**λ (nm)**	**E (eV)**	**f**	**Assignment**
$S_0 \rightarrow S_1$	609	2.036	1.02	HOMO→LUMO (98%)
$S_0 \rightarrow S_2$	452	2.743	0.18	H−1→LUMO (90%)
$S_0 \rightarrow S_3$	388	3.196	0.06	HOMO→L+1 (85%)
MD parameter	**298 K**	**318 K**	**MD parameter**	**298 K**
Coulomb-SR (kJ mol^{-1})	−168	−191	Coulomb-SR (kJ mol^{-1})	−168
Lennard-Jones-SR (kJ mol^{-1})	−54	−67	Lennard-Jones-SR (kJ mol^{-1})	−54
Total interaction (kJ mol^{-1})	−222	−258	Total interaction (kJ mol^{-1})	−222
H-bonds (avg. per frame)	2.3	2.0	H-bonds (avg. per frame)	2.3

➢ *Proposed Adsorption Mechanism*

Combining all strands of evidence, MB capture by GA-g-poly(NIPAM-co-AAc) proceeds primarily through electrostatic pairing between the delocalized MB^+ cation and ionized carboxylate sites, reinforced by hydrogen bonds to amide and hydroxyl groups and by π/dispersion contacts with the polymer backbone. The FTIR band shifts, the pH profile pivoting around pH_{p46}, the entropy-driven thermodynamics and the MD energy decomposition all converge on this same picture, while the LCST transition adds a physical squeeze-and-release lever unavailable to conventional rigid adsorbents.

IV. CONCLUSION

A dual-responsive GA-g-poly(NIPAM-co-AAc) hydrogel was synthesised by free-radical grafting and characterised by FTIR, XRD and FESEM, which confirmed its amorphous, porous network structure with the predicted amide and carboxyl functionalities. The maximum removal of 97% methylene blue was achieved at pH 8 using the gel with the equilibrium attained after 90 min following pseudo-second order kinetic and Langmuir-type monolayer adsorption at 318 K with a maximum capacity of 312.5 mg g^{-1}. Thermodynamic analysis revealed a spontaneous, endothermic and entropy-driven process and the LCST of the network (≈34 °C) offered a practical thermal handle: brief warming released most of the bound dye, permitting over 90% of the capacity to be retained after five reuse cycles with a selectivity coefficient approaching 18 against an anionic competitor. DFT/TD-DFT calculations characterised MB as a soft, extremely electrophilic cation whose positive potential blankets the heteroaromatic core, while 50 ns MD simulations ascribed the binding mostly to Coulomb attraction toward carboxylates with hydrogen-bonding and π-stacking assistance. The material thus combines high capacity with low-cost, switchable regeneration and is a viable candidate for the treatment of cationic-dye effluents.

REFERENCES

[1]. Khan I, Saeed K, Zekker I, Zhang B, Hendi AH, Ahmad A, et al. Review on methylene blue: its properties, uses, toxicity and photodegradation. Water. 2022;14(2):242.

[2]. Crini G. Non-conventional low-cost adsorbents for dye removal: A review. Bioresour Technol. 2006;97(9):1061–1085.

[3]. Katheresan V, Kansedo J, Lau SY. Efficiency of various recent wastewater dye removal methods: A review. J Environ Chem Eng. 2018;6(4):4676–4697.

[4]. Ahmed EM. Hydrogel: Preparation, characterization, and applications: A review. J Adv Res. 2015;6(2):105–121.

[5]. Schild HG. Poly(N-isopropylacrylamide): experiment, theory and application. Prog Polym Sci. 1992;17(2):163–249.

[6]. Haq MA, Su Y, Wang D. Mechanical properties of PNIPAM based hydrogels: A review. Mater Sci Eng C. 2017;79:842–855.

[7]. Zhang J, Peppas NA. Synthesis and characterization of pH- and temperature-sensitive poly(methacrylic acid)/poly(N-isopropylacrylamide) interpenetrating polymeric networks. Macromolecules. 2000;33(1):102–107.

[8]. Patel S, Goyal A. Applications of natural polymer gum arabic: A review. Int J Food Prop. 2015;18(5):986–998.

[9]. Paulino AT, Guilherme MR, Reis AV, Campese GM, Muniz EC, Nozaki J. Removal of methylene blue dye from an aqueous media using superabsorbent hydrogel supported on modified polysaccharide. J Colloid Interface Sci. 2006;301(1):55–62.

[10]. Parr RG, Yang W. Density-Functional Theory of Atoms and Molecules. New York: Oxford University Press; 1989.

[11]. Lagergren S. Zur Theorie der sogenannten Adsorption gelöster Stoffe. K Sven Vetenskapsakad Handl. 1898;24(4):1–39.

[12]. Ho YS, McKay G. Pseudo-second order model for sorption processes. Process Biochem. 1999;34(5):451–465.

[13]. Weber WJ, Morris JC. Kinetics of adsorption on carbon from solution. J Sanit Eng Div Am Soc Civ Eng. 1963;89(2):31–60.

[14]. Langmuir I. The adsorption of gases on plane surfaces of glass, mica and platinum. J Am Chem Soc. 1918;40(9):1361–1403.

[15]. Freundlich HMF. Über die Adsorption in Lösungen. Z Phys Chem. 1906;57:385–470.

[16]. Temkin MJ, Pyzhev V. Recent modifications to Langmuir isotherms. Acta Physiochim URSS. 1940;12:217–222.

[17]. Lima EC, Hosseini-Bandegharaei A, Moreno-Piraján JC, Anastopoulos I. A critical review of the estimation of the thermodynamic parameters on

adsorption equilibria. J Mol Liq. 2019;273:425–434.
[18]. Frisch MJ, Trucks GW, Schlegel HB, Scuseria GE, Robb MA, Cheeseman JR, et al. Gaussian 16, Revision C.01. Wallingford CT: Gaussian, Inc.; 2016.
[19]. Becke AD. Density-functional thermochemistry. III. The role of exact exchange. J Chem Phys. 1993;98(7):5648–5652.
[20]. Lee C, Yang W, Parr RG. Development of the Colle–Salvetti correlation-energy formula into a functional of the electron density. Phys Rev B. 1988;37(2):785–789.
[21]. Barone V, Cossi M. Quantum calculation of molecular energies and energy gradients in solution by a conductor solvent model. J Phys Chem A. 1998;102(11):1995–2001.
[22]. Parr RG, Szentpály L, Liu S. Electrophilicity index. J Am Chem Soc. 1999;121(9):1922–1924.
[23]. Parr RG, Pearson RG. Absolute hardness: companion parameter to absolute electronegativity. J Am Chem Soc. 1983;105(26):7512–7516.
[24]. Reed AE, Curtiss LA, Weinhold F. Intermolecular interactions from a natural bond orbital, donor–acceptor viewpoint. Chem Rev. 1988;88(6):899–926.
[25]. Abraham MJ, Murtola T, Schulz R, Páll S, Smith JC, Hess B, Lindahl E. GROMACS: High performance molecular simulations through multi-level parallelism from laptops to supercomputers. SoftwareX. 2015;1–2:19–25.
[26]. Jorgensen WL, Maxwell DS, Tirado-Rives J. Development and testing of the OPLS all-atom force field on conformational energetics and properties of organic liquids. J Am Chem Soc. 1996;118(45):11225–11236.
[27]. Dodda LS, Cabeza de Vaca I, Tirado-Rives J, Jorgensen WL. LigParGen web server: an automatic OPLS-AA parameter generator for organic ligands. Nucleic Acids Res. 2017;45(W1):W331–W336.
[28]. Jorgensen WL, Chandrasekhar J, Madura JD, Impey RW, Klein ML. Comparison of simple potential functions for simulating liquid water. J Chem Phys. 1983;79(2):926–935.
[29]. Bussi G, Donadio D, Parrinello M. Canonical sampling through velocity rescaling. J Chem Phys. 2007;126(1):014101.
[30]. Parrinello M, Rahman A. Polymorphic transitions in single crystals: A new molecular dynamics method. J Appl Phys. 1981;52(12):7182–7190.
[31]. Hess B, Bekker H, Berendsen HJC, Fraaije JGEM. LINCS: A linear constraint solver for molecular simulations. J Comput Chem. 1997;18(12):1463–1472.
[32]. Essmann U, Perera L, Berkowitz ML, Darden T, Lee H, Pedersen LG. A smooth particle mesh Ewald method. J Chem Phys. 1995;103(19):8577–8593.
[33]. Salleh MAM, Mahmoud DK, Karim WAWA, Idris A. Cationic and anionic dye adsorption by agricultural solid wastes: A comprehensive review. Desalination. 2011;280(1–3):1–13.
[34]. Tran HN, You SJ, Hosseini-Bandegharaei A, Chao HP. Mistakes and inconsistencies regarding adsorption of contaminants from aqueous solutions: A critical review. Water Res. 2017;120:88–116.